IL NUOVO CIMENTO **39 C** (2016) 405
DOI 10.1393/ncc/i2016-16405-8

COLLOQUIA: IWM-EC 2016

Equilibration chronometry

ALAN B. MCINTOSH(1)(*), ANDREA JEDELE(1)(2) and SHERRY J. YENNELLO(1)(2)
(1) *Cyclotron Institute, Texas A&M University - College Station, TX, USA*
(2) *Department of Chemistry, Texas A&M University - College Station, TX, USA*

received 10 January 2017

Summary. — We study neutron-proton equilibration in dynamically deformed atomic nuclei created in nuclear collisions. The two ends of the elongated nucleus are initially dissimilar in compositions and equilibrate on a sub-zeptosecond timescale following first-order kinetics. The technique of equilibration chronometry used to obtain this result enables new insight into the nuclear equation of state that governs many nuclear and astrophysical phenomena leading to the origin of the chemical elements.

1. – Background and motivation

The nuclear Equation of State (nEoS) relates the energy, temperature, density, pressure, and neutron-proton asymmetry for a strongly interacting system. The nEoS governs many aspects of astrophysics such as neutron star physics and the explosive death of stars [1-4]. In terrestrial environments the nEoS plays a strong role influencing the neutron skin thickness of heavy nuclei, collective excitations of nuclei and the dynamics of heavy ion collisions [5-7]. The density dependence of the asymmetry energy remains the least-constrained facet of the nEoS. Refining our description of nuclear material with exotic neutron-proton content would aid in understanding the origin of the elements and in characterizing the structure of neutron stars. For the last two decades, scientists have broadened our understanding of the nEoS of neutron-rich and neutron-poor material [8, 9].

One method to constrain the asymmetry energy involves multi-nucleon exchange between nuclei leading to neutron-proton (NZ) equilibration. Although there has been significant work focused on measuring the asymptotic composition of the nuclei [10-13], some experiments have probed the timescale of the NZ equilibration process. Important efforts in the '70s and '80s [14-19] established the timescale is in the range of 0.1–1.0 zs

(*) E-mail: amcintosh@comp.tamu.edu

(1 zeptosecond is 10^{-21} seconds). This was achieved by measuring isotopic composition of fragments as a function of either the energy dissipation or the separation orientation. The dissipation is related to the interaction time and can be estimated through a model. A recent measurement of a broad range of isotopes and energy dissipation is consistent with this timescale [20]. Similarly, the separation angle is proportional to the interaction time and can be calibrated via angular momentum. Recent measurements by Hudan *et al.* [21-24] employing this technique reported certain fragment compositions explicitly as a function of time, indicating that equilibration continues for as long as 4 zs, though the majority of the equilibration takes place within 1 zs.

In this paper, we report clear and direct evidence of NZ equilibration between nuclear prefragments on a sub-zeptosecond timescale. Equilibration chronometry is made possible by correlating the compositions of multiple fragments to their breakup orientation in an experiment with near-complete angular coverage and excellent isotopic resolution. With the present data, this technique allows us to examine the detailed evolution of the NZ composition with extremely fine resolution.

2. – Reaction mechanism

Heavy-ion reactions around the Fermi energy produce an excited projectile-like fragment (PLF*) and an excited target-like fragment (TLF*) in a predominantly binary interaction. As the PLF* and TLF* separate after the collision, a low-density neck of material forms between the two bodies. Both the PLF* and TLF* may be strongly elongated even before they separate due to collision dynamics. This stretching out of the nuclear material can be beyond the ability of the nuclear force to hold it together. Consequently, the neck ruptures, and the PLF* and TLF* emerge deformed along their axis of separation [25-27]. Due to the deformation, the PLF* is then likely to break up quickly along the direction of its deformation. The same is true of the TLF*, but as our detectors are optimized to measure the kinematic region near the PLF*, we focus on the breakup of the PLF* with the assumption that the same process occurs for the TLF* [26]. Breakup due to the strong deformation is referred to as dynamical decay, and this process exhibits a characteristic strongly-peaked angular distribution [27-29].

The low density of the neck is critical to understanding further details of the reaction mechanism. As the system tends to minimize its energy, the density variation within the nuclear system provides a venue for the asymmetry term in the nEoS to play a role. There is an energy penalty associated with the excess particles (neutrons) in the system, but this penalty is less at lower density, and so the asymmetry energy provides the driving force for a net flow of neutrons to the low-density neck. In this way, before the PLF* and TLF* ever separate, the neck between them is neutron rich at their expense. The neutron enrichment is observed most strikingly in the yield of free neutrons produced, but is still observed to significantly impact the isotopic distributions of nuclear clusters [30].

3. – Experiment

The experiment was conducted at the Texas A&M University Cyclotron Institute. A beam of ^{70}Zn @ 35 MeV/nucleon impinged on a ^{70}Zn target, and charged particles and neutrons from the reactions were measured in the NIMROD-ISiS array [31] with nearly 4π coverage. This detector provides excellent isotopic identification of charged particles up to $Z = 17$ in most detectors, and up to $Z = 21$ in some detectors [31, 32]. Ions are identified with better than unit resolutions from $Z = 1$ to $Z = 30$

(the atomic number of the beam). The combination of the large geometric coverage and the excellent isotopic resolution are crucial to observing the NZ equilibration process in detail. In contrast to previous work where the lighter fragment of a binary split was measured and interpreted as demonstrating equilibration with its heavy partner, in this work we make the simultaneous measurement of both reaction partners of a binary split. The comparison between the composition of the two fragments provides a powerful demonstration of NZ equilibration within a nuclear system.

4. – Analysis

To focus on the dynamical decay of the PLF*, we select events in which at least two charged particles were measured in NIMROD. Fragments were sorted by their atomic number Z and same-Z fragments were sorted by their mass number A. We refer to the fragment with the largest Z as the heavy fragment (HF) and the fragment with the second largest atomic number as the light fragment (LF). The HF was required to have an atomic number of at least 12 and the LF was required to have an atomic number of at least 3. Additionally, the total charge detected (in the HF, LF, and all other charged particles combined) was required to be at least 21 and not more than 32 to ensure that we are considering events where a significant fraction of the projectile is measured. This increases the likelihood that HF and LF are indeed the two largest daughters of the PLF*. Finally, we imposed the restriction that both HF and LF be isotopically identified. Since the energy of each particle is measured, the mass is determined, and the polar and azimuthal angles of each particle is known from the detector in which it was measured, the velocity vectors $\vec{v}_H$ and $\vec{v}_L$ in the laboratory rest frame can be calculated directly. From these, we then define the two-fragment center of mass velocity in the laboratory frame as $\vec{v}_{cm} = (m_H\vec{v}_H + m_L\vec{v}_L)/(m_H + m_L)$ and the relative velocity as $\vec{v}_{rel} = \vec{v}_H - \vec{v}_L$. Finally, the angle α between the two fragment center-of-mass velocity and the relative velocity is calculated from the dot product $\cos(\alpha) = \frac{\vec{v}_{cm}\cdot\vec{v}_{rel}}{|\vec{v}_{cm}||\vec{v}_{rel}|}$. From these quantities, along with the composition of each fragment $\Delta = \frac{N-Z}{A}$, all the results in the following section are obtained. The analysis was performed for all combinations of Z_H and Z_L. The results are similar for all combinations, and for brevity and clarity in this report we present the results of the analysis for one combination, namely $Z_H = 12$ and $Z_L = 7$.

5. – Results and discussion

In fig. 1, we present the velocity distributions of both fragments HF (red) and LF (blue) projected along the beam direction. The upper black dashed line at $0.27c$ represents the velocity of the beam and the lower black dashed line at $0.13c$ represents mid-velocity. Both velocity distributions lie predominantly above mid-velocity. This indicates that both fragments are daughters of the PLF* rather than the TLF*. The distribution for the HF is peaked slightly below beam velocity, which is consistent with it being the heavy residue of the PLF* after some damping from beam velocity. The distribution for the LF is peaked significantly below the HF. This is consistent with dynamical decay, where rather than being emitted isotropically the LF is emitted preferentially in the backward direction. This occurs due to deformation of the nuclear system by the entrance channel dynamics. Thus the distributions in fig. 1 are consistent with expectations for dynamical decay.

In fig. 2, we present the angular distributions $\cos(\alpha)$, where α is the angle between $\vec{v}_{cm}$ and $\vec{v}_{rel}$. As indicated by the inset cartoon, $\cos(\alpha) = 1$ corresponds to the LF

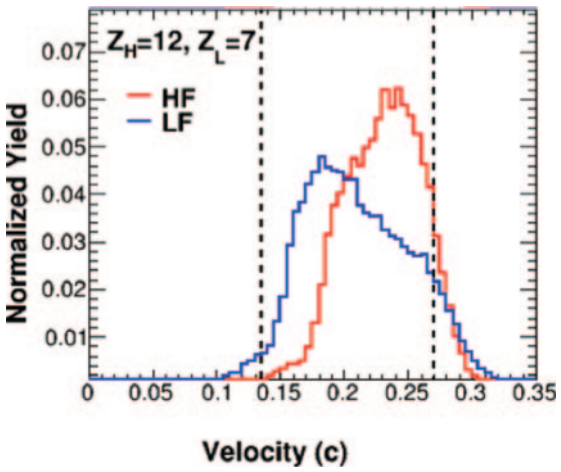

Fig. 1. – Velocity distributions, parallel to the beam axis, of the heaviest (HF) and second heaviest (LF) fragments found in each event. The absolute location of the distributions indicates that both fragments originate from the PLF*, and the relative location of the distributions indicates a significant dynamical yield. We focus on the case of $Z_H = 12$ and $Z_L = 7$; other fragments show the same physics.

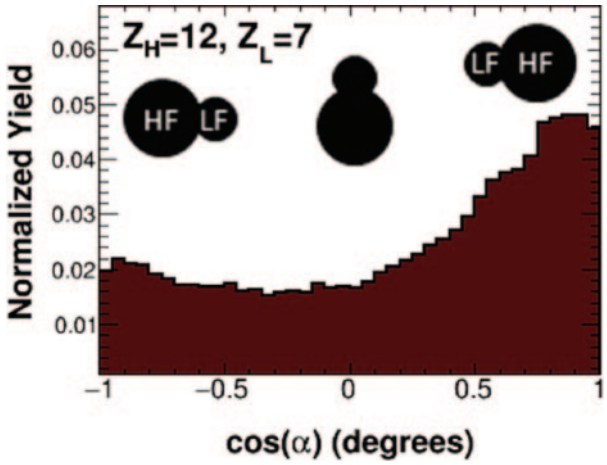

Fig. 2. – Distribution of the cosine of the rotational alignment angle α between $\vec{v}_{cm}$ and $\vec{v}_{rel}$. The yield toward cos(α)=1 corresponds to backward emission of the LF, *i.e.* from the PLF* back toward the TLF*. This excess backward yield is characteristic of dynamical decay. The measured degree of alignment when the PLF* decays combined with the angular velocity of the PLF* provides the basis for equilibration chronometry.

emitted backward relative to HF (*i.e.* toward lower velocity). The distribution is backward peaked, indicating that this emission orientation is preferred. Standard statistical decay from a source with no angular momentum would produce a flat cos(α) distribution. With finite angular momentum, the distribution increases in yield at the extremes cos(α) = $\pm$1 in a way that is symmetric about cos(α) = 0. The slight increase observed

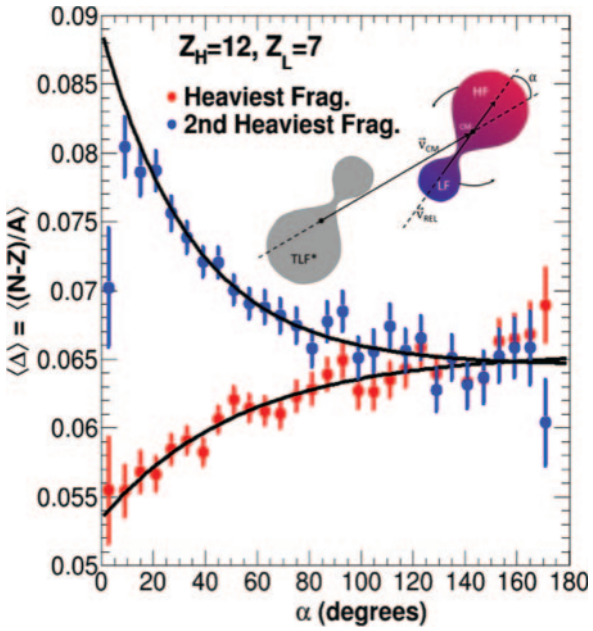

Fig. 3. – Relative neutron-proton composition Δ as a function of alignment α. The rotation of the the PLF* as indicated in the inset allows α to be interpreted as a time axis. The composition of the LF decreases exponentially at the same rate that the composition of the HF increases exponentially. This demonstrates equilibration within a nuclear system can be observed as a function of time, and that the equilibration follows first-order kinetics.

near $\cos(\alpha) = -1$ can therefore be a result of angular momentum, but this cannot account for the much larger yield peaked near $\cos(\alpha) = 1$. The effect of the detector acceptance was investigated with the help of the GEMINI++ model [33] and a software filter of the NIMROD-ISiS array. The forward/backward asymmetry in yield cannot be explained by the influence of the geometry, granularity, resolution, and thresholds of the detection device.

The excess yield near $\cos(\alpha) = 1$ is consistent with dynamical decay. The deformed system is likely to decay quickly along its deformation direction, that is to say $\vec{v}_{rel}$ is most likely to be along $\vec{v}_{cm}$. If some time elapses after the PLF*-TLF* split and before the PLF* splits into HF and LF, then the PLF* will rotate through some angle α determined by its angular momentum and moment of inertia. In order to observe this, the timescale of HF-LF decay must be short relative to the rotational period. Provided this ordering of timescales, the angle α can be used as a clock measuring the time between the PLF*-TLF* split and the breakup of the PLF* into HF and LF.

In fig. 3, we present the average composition Δ as a function of the alignment angle α. The composition for the HF is shown by the red circles, and the composition of the LF by the blue circles. The LF starts off quite neutron rich at time zero ($\alpha = 0$) and evolves to become less neutron rich. The HF starts off neutron poor at time zero and evolves to become more neutron rich. The evolution of each is well described by an exponential function. The black lines are fits of the form $\Delta = a + b\ \exp(-c\alpha)$. The c parameter represents a rate constant. The rate constants for HF and LF agree within statistical uncertainty.

The low density of the neck and the action of the symmetry energy ensure that the neck is neutron-rich before the PLF* and TLF* separate. After separation of the PLF* from the TLF*, the PLF* is deformed and has an abundance of neutrons on its smaller, trailing end. The PLF* may break into a HF and LF at some time. If it breaks promptly, the rotation angle will be 0°, and the composition of the LF will be much more neutron rich than the HF. If some time elapses between the PLF*-TLF* scission and the scission of the PLF* into HF and LF, then the PLF* will rotate through some angle α due to its angular momentum and some degree of neutron-proton equilibration can occur between the regions of the PLF*. This scenario is illustrated by the cartoon inset in fig. 3.

The qualitative expectations of this equilibration scenario match the measurement shown in fig. 3. From the data, we conclude the following things. First, the rotational period of the PLF* is longer than the equilibration time scale, but not vastly so, which allows the angle to be used effectively as a clock. Second, the initial condition at the time of PLF*-TLF* scission is for the neck to be neutron rich. Third, the equilibration is observed to occur as time progresses as evidenced by the change in the composition of the LF and also as evidenced for the first time by the contemporaneous change in the composition of the HF. Fourth, the data are of sufficient quality that the shape of the equilibration curves can be ascertained also for the first time. Fifth, equilibration curves follow exponential trends, providing the first experimental evidence that NZ equilibration follows first-order kinetics.

6. – Summary

Thus we have for the first time direct experimental evidence of NZ equilibration occurring between two reaction partners. Moreover, with this technique, we are able to observe the equilibration as a function of time through the rotation angle α. Work is already in progress to calibrate α in terms of time, which will allow extraction of the true rate constants for NZ equilibration. The examination of the time-dependence of the equilibration provides a link to the nEoS. A previously unobserved facet of the nEoS is that NZ equilibration follows first order kinetics.

In 2004, Tsang *et al.* [10] published nucleon transport simulations that displayed sensitivity of NZ equilibration to the form of the density dependence of the asymmetry energy employed in the model. A plot of the composition of the reaction partners changing with time illustrated that equilibration depends on the contact time, the potential driving equilibration, and the relative NZ asymmetry of the reaction partners. Subsequent research focused on how the final-state nuclear compositions might be used to constrain the nEoS rather than on measuring the time dependence of the equilibration. However, the time dependence carries more information about the nEoS than the final-state values, and our current results demonstrate that this can be observed with the proper tools. This new data, and the new avenue of experimental research it opens up, will guide theoretical developments in nuclear science. These advances promise to deepen our understanding of the fundamental interactions of nuclear material.

* * *

This work was supported by the Robert A. Welch Foundation (Grant A-1266) and the United States Department of Energy (Grant DE-FG02-93ER40773).

REFERENCES

[1] Demorest P. B. *et al.*, *Nature*, **467** (2010) 1081.
[2] Steiner A. W. *et al.*, *Phys. Rep.*, **411** (2005) 325.
[3] Lattimer J. M. and Prakash M., *Astrophys. J.*, **550** (2001) 426.
[4] Lattimer J. M. and Prakash M., *Science*, **304** (2004) 536.
[5] Garg U. *et al.*, *Nucl. Phys. A*, **788** (2007) 1.
[6] Baran V. *et al.*, *AIP Conf. Proc.*, **1645** (2015) 267.
[7] Roca-Maza X. *et al.*, *Phys. Rev. Lett.*, **106** (2011) 252501.
[8] Horowitz C. J. *et al.*, *J. Phys. G*, **41** (2014) 093110.
[9] Tsang M. B. *et al.*, *Phys. Rev. C*, **86** (2012) 015803.
[10] Tsang M. B. *et al.*, *Phys. Rev. Lett.*, **92** (2004) 062701.
[11] Shetty D. V. *et al.*, *Phys. Rev. C*, **76** (2007) 024606.
[12] Sun Z. Y. *et al.*, *Phys. Rev. C*, **82** (2010) 051603.
[13] May L. W., PhD Thesis, Texas A&M University (2015).
[14] Galin J. *et al.*, *Z. Phys. A*, **278** (1976) 347.
[15] Kratz J. V. *et al.*, *Phys. Rev. Lett.*, **39** (1977) 984.
[16] Moretto L. G. and Schmitt R. P., *Rep. Prog. Phys.* , **44** (1981) 533.
[17] Hernandez E. S. *et al.*, *Nucl. Phys. A*, **361** (1981) 483.
[18] Matthews G. J. *et al.*, *Phys. Rev. C*, **25** (1982) 300.
[19] Freisleben H. and Kratz J. V., *Phys. Rep.*, **601** (1984) 1.
[20] Souliotis G. A. *et al.*, *Phys. Rev. C*, **90** (2014) 064612.
[21] Hudan S. *et al.*, *Phys. Rev. C*, **86** (2012) 021603.
[22] Brown K. *et al.*, *Phys. Rev. C*, **87** (2013) 061601.
[23] Steifel K. *et al.*, *Phys. Rev. C*, **90** (2014) 061605.
[24] Hudan S. and deSouza R. T., *Eur. Phys. J. A*, **50** (2014) 36.
[25] Montoya C. P. *et al.*, *Phys. Rev. Lett.*, **73** (1994) 3070.
[26] Colin J. *et al.*, *Phys. Rev. C*, **67** (2003) 043603.
[27] McIntosh A. B. *et al.*, *Phys. Rev. C*, **81** (2010) 034603.
[28] Bocage F. *et al.*, *Nucl. Phys. A*, **676** (2000) 391.
[29] Davin B. *et al.*, *Phys. Rev. C*, **65** (2002) 064614.
[30] Theriault D. *et al.*, *Phys. Rev. C*, **74** (2006) 051602(R).
[31] Wuenschel S. *et al.*, *Nucl. Instrum. Methods A*, **604** (2009) 578.
[32] Kohley Z. W. *et al.*, *Phys. Rev. C*, **82** (2010) 064601.
[33] Charity R. J. *et al.*, *Phys. Rev. C*, **74** (1998) 051602.